Inorganic Chemistry

ARTICLE

pubs.acs.org/IC

Uniform Hollow Lu_2O_3:Ln (Ln = Eu^{3+}, Tb^{3+}) Spheres: Facile Synthesis and Luminescent Properties

Piaoping Yang,[†] Shili Gai,[†] Yanchao Liu,[†] Wenxin Wang,[†] Chunxia Li,[‡] and Jun Lin*[,‡]

[†]The Key Laboratory of Superlight Materials and Surface Technology, Ministry of Education, Harbin Engineering University, Harbin 150001, P. R. China

[‡]State Key laboratory of Rare Earth Rear Resource Utilization, Changchun Institute of Applied Chemistry, Chinese Academy of Sciences, Changchun 130022, P. R. China

ABSTRACT: Uniform hollow Lu_2O_3:Ln (Ln = Eu^{3+}, Tb^{3+}) phosphors have been successfully prepared via a urea-assisted homogeneous precipitation method using carbon spheres as templates, followed by a subsequent calcination process. X-ray diffraction (XRD), scanning electron microscopy (SEM), transmission electron microscopy (TEM), Fourier transformed infrared (FT-IR), thermogravimetric and differential thermal analysis (TG-DTA), photoluminescence (PL) spectra, cathodoluminescence (CL) spectra, kinetic decays, quantum yields (QY), and UV−visible diffuse reflectance spectra were employed to characterize the samples. The results show that hollow Lu_2O_3:Ln spheres can be indexed to cubic Gd_2O_3 phase with high purity. The as-prepared hollow Lu_2O_3:Ln phosphors are confirmed to be uniform in shape and size with diameter of about 300 nm and shell thickness of approximate 20 nm. The possible formation mechanism of evolution from the carbon spheres to the amorphous precursor and to the final hollow Lu_2O_3:Ln microspheres has been proposed. Upon ultraviolet (UV) and low-voltage electron beams excitation, the hollow Lu_2O_3:Ln (Ln = Eu^{3+}, Tb^{3+}) spheres exhibit bright red (Eu^{3+}, $^5D_0-^7F_2$) and green (Tb^{3+}, $^5D_4-^7F_5$) luminescence, which may find potential applications in the fields of color display and biomedicine.

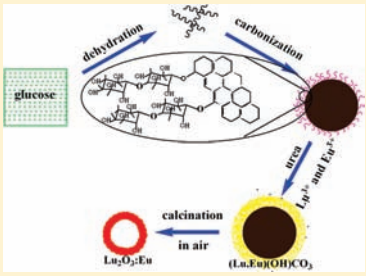

1. INTRODUCTION

The development of nanocrystals with controllable size and morphology has been extensively pursued, not only for their fundamental scientific interest, but also for their technological applications.[1] Among all these nanocrystals, hollow colloidal particles are exceptionally promising materials in diverse fields of technology including catalysis,[2] drug delivery,[3] photonics,[4] biotechnology,[5] fillers (or pigment/coatings),[6] protection of biologically active agents,[7] and electrochemical cells.[8] During the past decades, much effort has been exerted in the development of different methods for the design and fabrication of the hollow structured spheres, such as heterophase polymerization combined with the sol−gel process,[9] emulsion/interfacial polymerization strategies,[10] gas bubble assisted approach,[11] spray-drying method,[12] self-assembly technique,[13] and layer-by-layer method.[14]

Besides these methods, template method has been widely applied to fabricate hollow spheres.[15] In a typical procedure, template particles are coated by surface absorption or precipitation of inorganic precursors to form core−shell structured composites. The template cores are subsequently removed by selective reaction in an appropriate solvent or by calcination at desired temperatures and atmosphere to create hollow spheres. Of all the templates, monodisperse polymer latex and silica spheres are commonly used as colloidal templates because they are readily available in a wide range of sizes.[16] Recently, other colloidal systems have been developed which expanded the range of core materials applied for the sacrifice template method, such as resin,[17] biotemplates (yeast cell, ferritin, spherobacterium, and bacteria),[18] and liquid droplets.[19]

Because of the interesting physical properties of the lutetium oxide, such as high melting point, phase stability, and low thermal expansion,[20] it always serves as an excellent candidate for lanthanide ion substitution. Also, lutetium (Lu) may be a more favorable cation than yttrium (Y) for trivalent lanthanide dopant emission due to the intensity-borrowing mechanism mixing the 4f and 5d orbitals of the Ln^{3+} ions via the lattice valence band levels.[21] Furthermore, rare earth doped Lu_2O_3 phosphors should be one of the most perspective materials for X-ray detection and imaging due to the high effective atomic number (Z = 71) and its extremely high density (ρ = 9.42 g/cm^3) in comparison with Y_2O_3 (ρ = 4.8 g/cm^3) and Gd_2O_3 (ρ = 7.6 g/cm^3). And the research on the fabrication of Lu_2O_3 phosphors has been extensively carried out. For example, one-dimensional Lu_2O_3 phosphors and three-dimensional flower-like Lu_2O_3 have been synthesized through the hydrothermal methods.[22] Two-dimensional Lu_2O_3 epitaxial films have also been fabricated via pulsed-laser deposition.[23] The single-crystalline and monodisperse cubic Lu_2O_3 nanocrystals were reported via a nonhydrolytic approach in oleic acid/oleylamine/1-octadecene using various rare-earth complexes.[24] However, the study on the synthesis of hollow Lu_2O_3:Ln phosphors has rarely been reported. Furthermore, some of the methods mentioned above are complex and not easy

Received: August 8, 2010
Published: February 16, 2011

dx.doi.org/10.1021/ic101605k | *Inorg. Chem.* 2011, 50, 2182–2190

to control the morphology of the products. Hence, it is specially promising to develop a simple and green approach to prepare hollow Lu_2O_3:Ln phosphors.

Herein, we proposed a facile process for the synthesis of uniform Lu_2O_3:Ln hollow microspheres using urea as precipitating agent and colloidal carbon spheres as templates, followed by a further heat-treating process. Different from colloidal melamine formaldehyde (MF), microspheres with the particle size of 2.3 μm were used as template, which resulted in the large particle size (about 2 μm) of the final Y_2O_3:Ln phosphors;[16c] uniform and monodisperse carbon microspheres with less than 350 nm diameter were employed as the sacrifice template. Thus, the obtained fluorescent Lu_2O_3:Ln microspheres exhibit much smaller particle size. The approach has been proved to be a green route without using an organic template and any etching process, where the corrosive acid or base are usually used as the etching agents. In particular, the method are suitable for high-yield mass production of hollow Lu_2O_3:Ln phosphors with controllable properties, based on its simple and environmentally friendly preparation process. A possible formation mechanism was also proposed as well.

2. EXPERIMENTAL SECTION

2.1. Materials. All materials were used as received including analytical grade glucose, urea, and dilute HNO_3 (Beijing Chemical Corporation), Lu_2O_3 (99.99%), Eu_2O_3 (99.99%), and Tb_4O_7 (99.99%) (Science and Technology Parent Company of Changchun Institute of Applied Chemistry).

2.2. Preparation of Carbon Microspheres. The carbon microspheres templates were prepared through the poly condensation reaction of glucose under hydrothermal conditions. In a typical procedure, glucose (8 g) was dissolved in 40 mL of deionized water to form a clear solution. The solution was then sealed in a 50 mL Teflon-lined stainless autoclave and maintained at 170 °C for 9 h. After the autoclave was naturally cooled to room temperature, the black−brown precipitates were obtained and washed with deionized water six times then dried at 80 °C for 6 h in air.

2.3. Synthesis of Hollow Lu_2O_3:Eu^{3+} and Lu_2O_3:Tb^{3+} Microspheres. In a typical process for the synthesis of hollow Lu_2O_3:Eu^{3+} spheres with an Eu^{3+} doping concentration of 5 mol % with respect to Lu^{3+}, 0.475 mmol of Lu_2O_3 and 0.025 mmol of Eu_2O_3 were dissolved in 2 mol L^{-1} of HNO_3 with stirring. The superfluous HNO_3 was driven off by heating until the pH value of the solution reached between 2 and 3. The as-prepared $Lu(NO_3)_3$ and $Eu(NO_3)_3$ were added to 30 mL of deionized water. Then 3.0 g of urea was dissolved in the solution under vigorous stirring to form a clear solution. The as-prepared carbon microspheres (100 mg) were then added into above solution under ultrasonication for 15 min. Finally, the mixture was transferred into a 100 mL flask and heated at 90 °C for 4 h with vigorous stirring before the product was collected by centrifugation. The precursors were washed by deionized water and ethanol three times and dried at 60 °C in air. The final hollow Lu_2O_3:Eu^{3+} spheres were obtained through a heat treatment at 800 °C in air for 2 h with a heating rate of 2 °C min^{-1}. Hollow Lu_2O_3:Tb^{3+} microspheres with Tb^{3+} doping concentration of 2 mol % were prepared via the same procedure. For comparison, nanosolid Lu_2O_3:Eu^{3+} and Lu_2O_3:Tb^{3+} particles with the same doping compositions were obtained by a similar urea-assisted precipitation and further calcination process except that no carbon microspheres were added. Moreover, bulk Lu_2O_3:Eu^{3+} and Lu_2O_3:Tb^{3+} phosphors were prepared by heating the corresponding rare earth nitrates at 800 °C in air for 2 h.

2.4. Characterization. X-ray diffraction (XRD) was examined on a Rigaku-Dmax 2500 diffractometer using Cu Kα radiation (λ = 0.15405 nm).

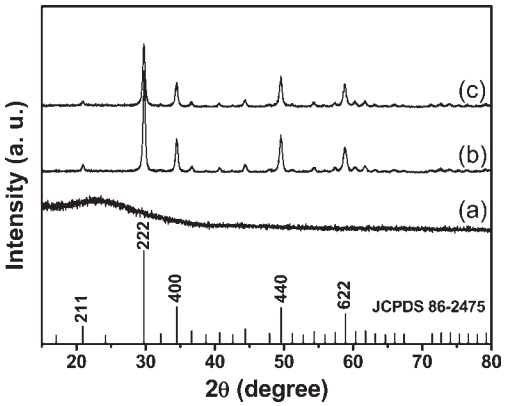

Figure 1. XRD patterns of the precursor (a), hollow Lu_2O_3:Eu^{3+} spheres (b), hollow Lu_2O_3:Tb^{3+} spheres (c), and the standard data for cubic Lu_2O_3 structure (JCPDS no. 86-2475).

The morphologies and composition of the as-prepared samples were inspected on a field emission scanning electron microscope (FE-SEM, S4800, Hitachi) equipped with an energy-dispersive X-ray spectrum (EDS, JEOL JXA-840). Transmission electron microscope (TEM) and high-resolution transmission electron microscope (HRTEM) were performed on a FEI Tecnai G^2 S-Twin transmission electron microscope with a field emission gun operating at 200 kV to elucidate the dimensions and the structural details of the particles. Fourier-transform IR (FT-IR) spectra were measured on a Perkin-Elmer 580B IR spectrophotometer using KBr pellet technique. Thermogravimetry (TG) and differential thermal analysis (DTA) were carried out on a Netzsch STA 409 thermoanalyzer with a heating rate of 5 °C min^{-1}. The excitation and emission spectra were obtained on a Hitachi F-4500 spectrophotometer equipped with a 150 W xenon lamp as the excitation source. Luminescence decay curves were obtained from a Lecroy Wave Runner 6100 Digital Oscilloscope (1 GHz) using a 250 nm laser (pulse width = 4 ns, gate = 50 ns) as the excitation source (Continuum Sunlite OPO). The cathodoluminescent (CL) measurements were carried out in an ultrahigh-vacuum chamber (10^{-8} Torr), where the phosphors were excited by an electron beam at a voltage range of 1−5 kV, and the spectra were recorded using an F-4500 spectrophotometer. Photoluminescence quantum yields (QYs) was measured by a C9920-02 absolute PL quantum yield measurement system from Hamamatsu. UV−visible diffuse reflectance spectra (UV-DRS) were carried out on a Shimadzu UV-3100 spectrophotometer. All the measurements were performed at room temperature.

3. RESULTS AND DISCUSSION

3.1. Phase, Structure, and Morphology. Figure 1 shows the X-ray diffraction patterns of the as-prepared precursor, hollow Lu_2O_3:Eu^{3+} and Lu_2O_3:Tb^{3+} microspheres, and the standard peak positions of cubic Lu_2O_3 (JCPDS no. 86-2475) as a reference. In Figure 1a for the uncalcined precursor, a broad peak at about 2θ = 22° suggests the amorphous nature of the uncalcined precursor. Hence, it can be inferred that the calcination process has a dual function: the formation of hollow crystalline structures from the amorphous precursor layer and elimination of carbon spheres cores. As for the hollow Lu_2O_3:Eu^{3+} and Lu_2O_3:Tb^{3+} spheres (Figure 1b and c), all the diffraction peaks can be directly indexed to the cubic Lu_2O_3 phase (*Ia*3 space group) according to the standard card (JCPDS no. 86-2475). No traces of additional peaks from the doped components can be detected, implying the high purity of the two samples. The calculated lattice constants, the deviations, and the

Table 1. Unit Cell Lattice Constants, Crystallite Sizes, and Quantum Yields (QYs) for Hollow $Lu_2O_3:Eu^{3+}$ and $Lu_2O_3:Tb^{3+}$ Microspheres

samples	a/deviation (Å)	cell volume/deviation (nm^3)	crystallite size (nm)	quantum yields (%)
JCPDS no. 86-2475	10.391	1.122		
$Lu_2O_3:Eu^{3+}$	10.401/0.01	1.128/0.006	21.3	19.8
$Lu_2O_3:Tb^{3+}$	10.407/0.016	1.133/0.011	17.8	4.4

crystallite sizes of the two samples are summarized in Table 1, and the standard data of cubic Lu_2O_3 (JCPDS no. 86-2475) are listed for comparison. It can be seen that the calculated lattice constants for the hollow $Lu_2O_3:Eu^{3+}$ and $Lu_2O_3:Tb^{3+}$ spheres correspond well to the standard data. The slightly enlarged lattice constants can be related with the larger ion radius of the doped rare earth ions. The average crystallite sizes of hollow Lu_2O_3:Ln spheres can be calculated from the Scherrer formula: $D_{hkl} = K\lambda/(\beta \cos \theta)$, where λ is the X-ray wavelength (0.15405 nm), β is the full width at half-maximum, θ is the diffraction angle, K is a constant (0.89), and D_{hkl} means the size along the (hkl) direction. The strongest three peaks (222) at $2\theta = 29.76°$, (400) at $2\theta = 34.49°$, and (440) at $2\theta = 49.58°$ were used to calculate the average crystallite sizes (D) of the samples. The estimated crystal size of $Lu_2O_3:Eu^{3+}$ and $Lu_2O_3:Tb^{3+}$ are calculated to be 21.3 and 17.8 nm, respectively.

Figure 2 shows SEM and TEM images of the as-prepared carbon spheres. It can be seen from the SEM image (Figure 2a) that the sample consists of monodisperse microspheres with smooth surface and narrow size distribution in the range of 300−350 nm. The sizes of carbon spheres can be tuned by altering the reaction temperature, reaction time, and concentration of starting materials.[25] The size of final hollow phosphors should therefore be tuned by employing carbon spheres with different sizes as templates.

The morphology and the microstructure details of the as-prepared precursor before calcination were examined with SEM and TEM techniques, as shown in Figure 3. It can be seen that the precursor particles still keep the spherical morphology of the as-prepared carbon spheres except for a slightly larger particle size, which should be clearly due to the coated $Lu(OH)CO_3$ shell (this conclusion can be found from the FT-IR spectra). Additionally, it should be noted that the precursor particles exhibit a much rougher surface than the bare carbon spheres due to the urea-based precipitation of a large number of nanoparticles, which can be clearly observed from the high-magnification SEM (Figure 3b) and TEM (Figure 3e) images. The energy-dispersive X-ray spectrum (EDS, Figure 3c) confirms the strong signal of carbon, oxygen, europium, and lutetium in the product. From the TEM images (Figure 3d and e), it can be seen that the precursor particles consist of rough surface microspheres in the size range of 370−430 nm, which are similar to the SEM results. Furthermore, the core−shell structure can be clearly seen, which may be due to the coated $Lu(OH)CO_3$ layer on the surface of the carbon spheres.

Figure 4 displays the morphology, microstructure and the elemental composition of the hollow $Lu_2O_3:Eu^{3+}$ microspheres. From the low-magnification SEM image (Figure 4a) and the low-magnification TEM image (Figure 4d), it is apparent that the product consists of relatively uniform, well-dispersed hollow microspheres with a size range of 250−300 nm and shell thickness of about 20 nm, implying the carbon sphere templates essentially determine the shape and size of the final hollow phosphors. It is also clear that the hollow $Lu_2O_3:Eu^{3+}$ spheres

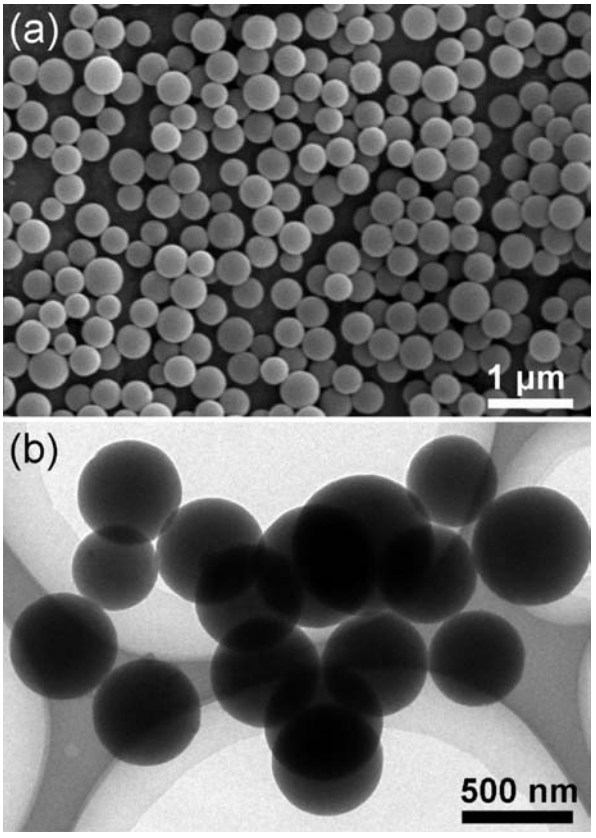

Figure 2. FE-SEM image (a) and TEM image (b) of as-prepared carbon spheres.

show obviously decreased particle size in comparison with the as-prepared precursor spheres, which may be assigned to the shrinkage by the dehydration of the cross-linked structure of carbon templates and crystallization of Lu_2O_3 phase from the loosely covered precursor during the calcination process. Additionally, in the high-magnification SEM (indicated by the arrow, Figure 4b), the ruptured hollow microsphere indicates the hollow structure of the final product, which may be caused by the release of CO_2 during the phase transformation process. The EDS analysis in Figure 4c confirms the presence of the oxygen, europium, and lutetium. It should be pointed out that the very weak carbon signal in the EDS suggests that the carbon core has nearly been burned off after the calcination process. Moreover, from the EDS of hollow $Lu_2O_3:Eu^{3+}$ spheres, the atomic ratio of the sample (O/(Lu + Eu) = 1.49/1) can be calculated, which is in good agreement with the stoichiometric atomic ratio of the $Lu_2O_3:Eu^{3+}$ sample. From the TEM images (Figure 4d and e), the strong contrast between the dark edge and the pale center evidence the hollow structure of $Lu_2O_3:Eu^{3+}$, and the sizes of the hollow spheres are very consistent with the SEM result. The low-magnification TEM image (Figure 4d) also shows some incomplete $Lu_2O_3:Eu^{3+}$ shell structure, which may be due to the

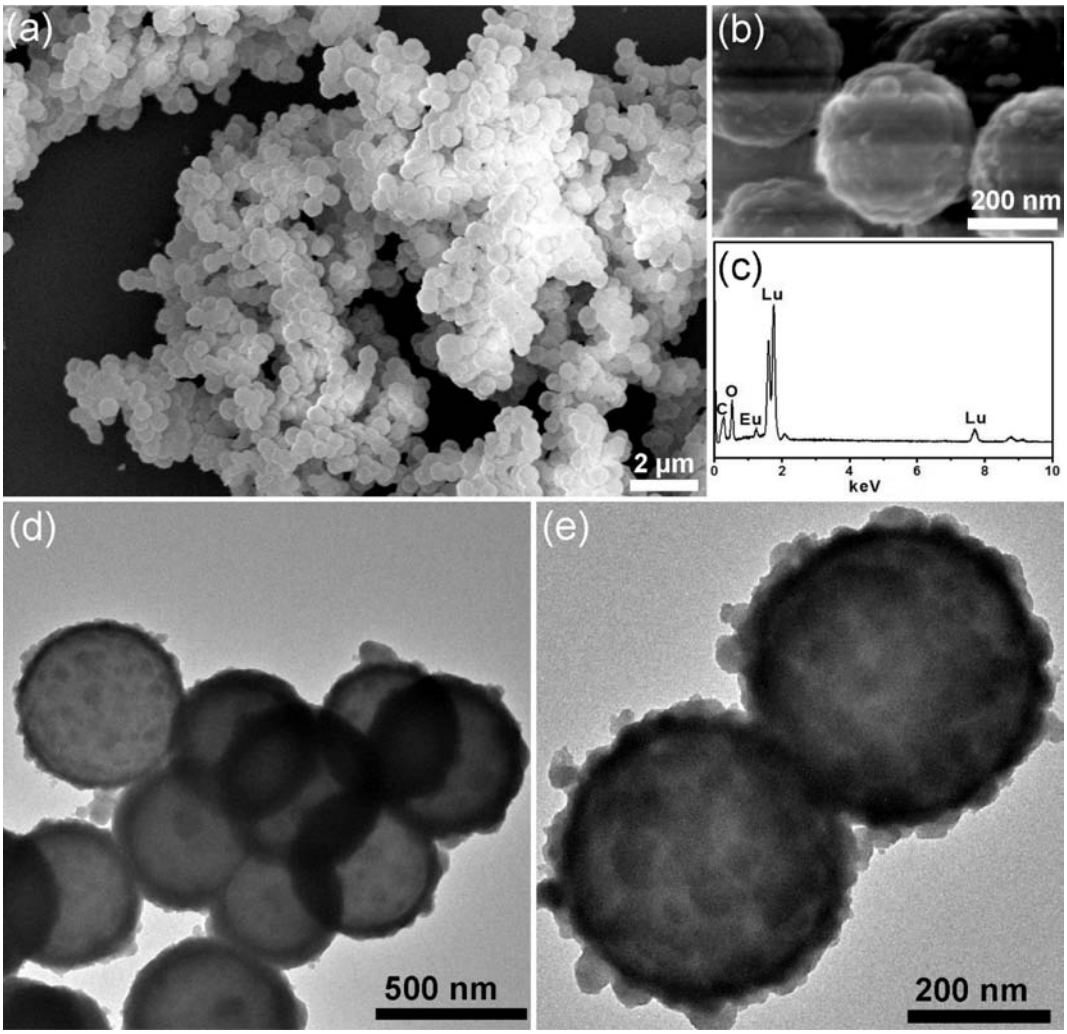

Figure 3. FE-SEM images of the uncalcined precursor (a), high magnification SEM image (b), EDS of uncalcined precursor (c), TEM image of uncalcined precursor (d), and high-magnification TEM image (e).

escapement of the carbon dioxide in the process of calcination. The thickness of the Lu_2O_3:Eu shell structure can be detected to be 20−25 nm in Figure 4e. In fact, the thickness of the shell can be tuned by adjusting the fabrication conditions, such as reaction temperature, reaction time, and the concentrations of the starting materials coated on carbon spheres. Additionally, the thickness of the coated phosphors should also be related with the sizes of the carbon spheres, which could be tuned by altering the synthetic conditions and glucose concentrations. In the corresponding selected area electron diffraction (SAED) (Figure 4f), the clear concentric rings from inside to outside can be directly indexed to (222), (400), (440) and (622) planes of the cubic Lu_2O_3 phase, demonstrating the polycrystalline nature of the hollow Lu_2O_3:Eu^{3+} spheres. Moreover, the lattice fringes in the HRTEM image (Figure 4g) also confirm the high crystallinity of the product.

The conversion process from the $Ln(OH)CO_3$ precursor to the final hollow Lu_2O_3:Eu^{3+} spheres during calcination was explored via TG-DTA, as shown in Figure 5a (the inset is the corresponding DTA). The TG curve of $Ln(OH)CO_3$ precursor can be mainly divided into three stages. The weight loss before 150 °C should be due to the physically adsorbed water on the surface of the product. The second slow weight loss with a maximum peak at 318 °C can be attributed to the dehydration and densification of the carbon spheres core. And the burning of the carbon sphere templates and the decomposition of the $Ln(OH)CO_3$ precursor should result in the weight loss between 410 and 500 °C. Seen from Figure 5b for pure carbon spheres, the final weight loss of carbon spheres is almost 100%, revealing that the carbon spheres can be totally removed by heating treatment. While for the lutetium composite precursor (Figure 5a), the total weight loss is determined to 69.5%, which is very consistent with calculated results according to the amount of starting materials. The results also reveal the high yield of the hollow phosphors obtained by this method.

The functional groups on the carbon spheres, the uncalcined precursor, and the hollow Lu_2O_3:Eu^{3+} spheres were examined by the FT-IR spectra, as shown in Figure 6. The FT-IR spectrum of the carbon spheres (Figure 6a) shows the peaks corresponding to functionalities including hydroxyl (3419 cm^{-1}), carbonyl (1702 cm^{-1}), unsaturated C═C (1620, 1507 cm^{-1}), —C—OH (1217 cm^{-1}), and glycosidic —C—O—C— linkage (1019 cm^{-1}). The presence of glycosidic linkage confirms the polymerization reaction of glucose, and the unsaturated C═C groups indicate that a carbonization process has occurred during the formation process of carbon spheres. The hydroxyl groups on the surface improve the stability of the carbon spheres in aqueous

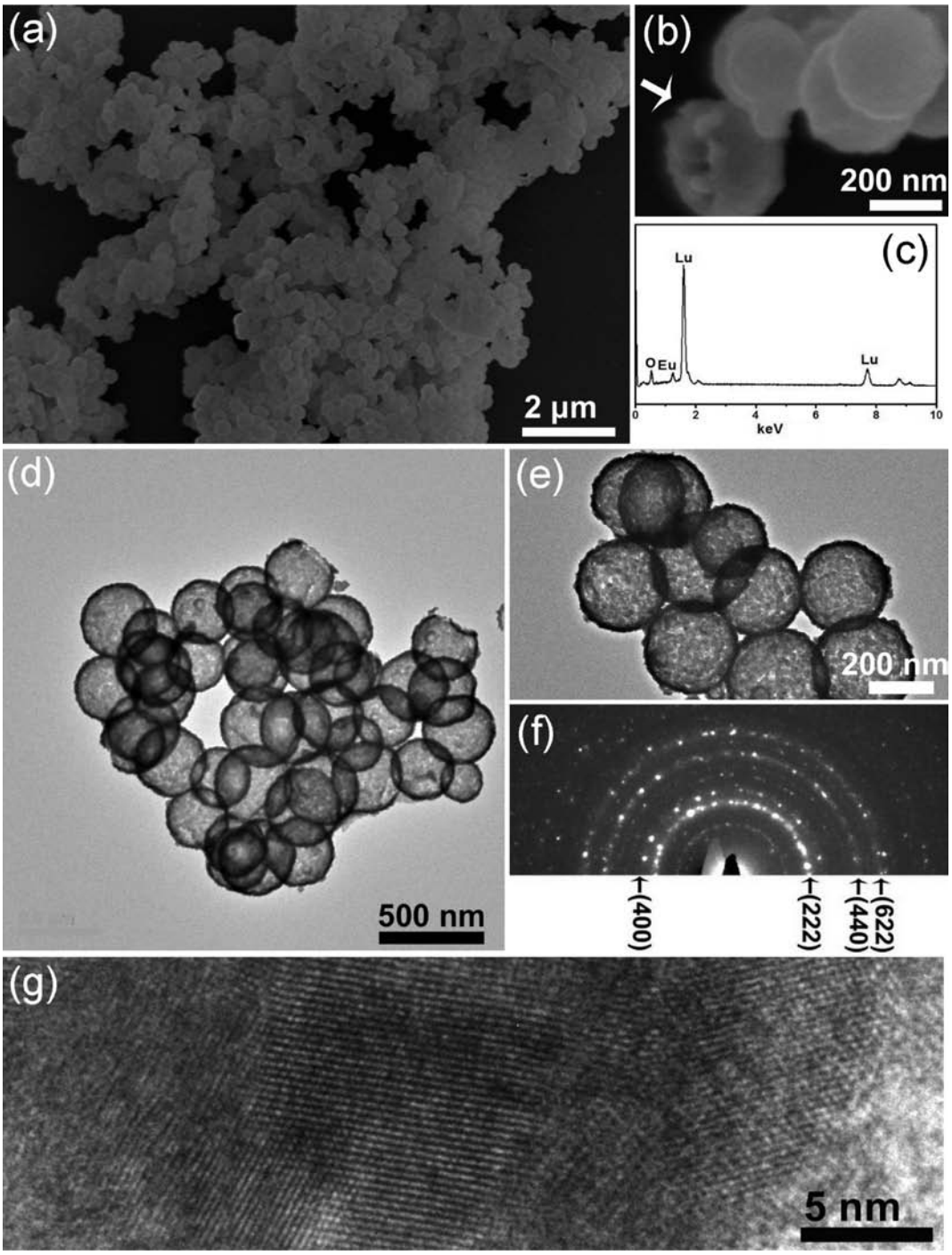

Figure 4. FE-SEM images of hollow $Lu_2O_3:Eu^{3+}$ spheres (a), high-magnification SEM image (b), EDS of $Lu_2O_3:Eu^{3+}$ (c), TEM images of hollow $Lu_2O_3:Eu^{3+}$ spheres (d), high-magnification TEM image (e), SAED (f), and HRTEM image (g) of hollow $Lu_2O_3:Eu^{3+}$ spheres.

solution, which can be identified by the SEM result. In the FTIR spectrum for the uncalcined precursor (Figure 6b), the respective adsorption band at about 3411, 1392, 1518, 1071, and 845 cm^{-1} can be assigned to OH (υ), CO (υ_{as}), CO (υ_{as}), CO (υ_s), and CO (δ) (υ = stretch; υ_s = symmetric stretch; υ_{as} = asymmetric stretch; δ = deformation), suggesting the composition of the precursor. Figure 6c shows the FT-IR spectrum of the hollow $Lu_2O_3:Eu^{3+}$ spheres. It can be seen that almost all the functional groups related with the carbon spheres and the precursor disappear, revealing the complete removal of carbon template and the transformation from the precursor to the hollow structured product. Furthermore, a new band at 573 cm^{-1} can be assigned to the Lu(Eu)−O stretching adsorption, which also confirms the formation of hollow Lu_2O_3:Ln spheres via the urea-based precipitation and the further annealing process.

3.2. Luminescent Properties. The hollow $Lu_2O_3:Eu^{3+}$ and $Lu_2O_3:Tb^{3+}$ microspheres exhibit bright red and green emission under ultraviolet (254 nm) irradiation (inset in Figure 7), respectively. Figure 7 also gives the PL excitation and emission

dx.doi.org/10.1021/ic101605k |*Inorg. Chem.* 2011, 50, 2182–2190

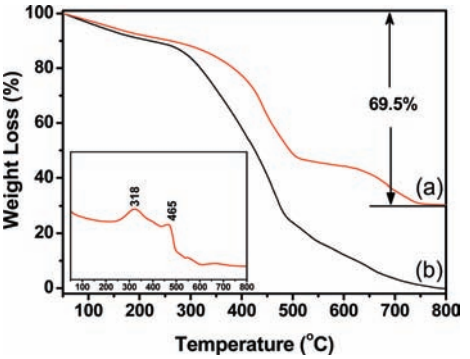

Figure 5. TG curves of as-prepared uncalcined precursor (a) and carbon spheres (b). (inset) Corresponding DTA curve of the uncalcined precursor in part a.

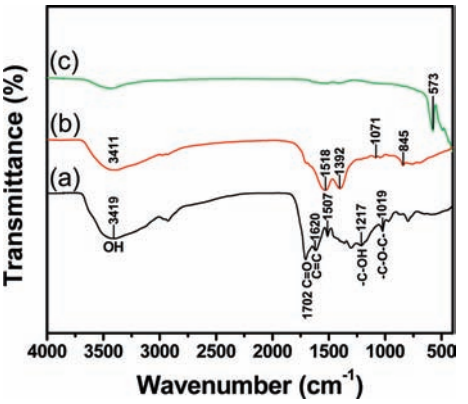

Figure 6. FT-IR of as-prepared carbon spheres (a), uncalcined precursor (b), and hollow Lu_2O_3:Eu^{3+} spheres (c).

spectra of the Lu_2O_3:Eu^{3+} and Lu_2O_3:Tb^{3+} samples, respectively. In the excitation spectrum (Figure 7a, left) monitored by the Eu^{3+} $^5D_0-^7F_2$ transition at 613 nm for hollow Lu_2O_3:Eu^{3+} spheres, the broad band with a maximum at 258 nm originates from the excitation of the oxygen-to-europium charge transfer band (CTB) and some very weak peaks in the longer-wavelength region are ascribed to the f−f transitions of the Eu^{3+} ions. Upon excitation at 258 nm, the emission spectrum (Figure 7a, right) of hollow Lu_2O_3:Eu^{3+} sample consists of the characteristic transition lines between Eu^{3+} levels. The locations and their assignments of the emission lines are labeled in the figure as well. The emission spectrum exhibits four main groups of emission lines at 538, 593, 613, and 649 nm, which are assigned to the $^5D_1-^7F_1$ and $^5D_0-^7F_J$ (J = 1, 2, 3) transitions of Eu^{3+}, respectively. Obviously, the emission spectrum is dominated by the red $^5D_0-^7F_2$ (613 nm) transition of the Eu^{3+}, which is an electric-dipole-allowed transition and hypersensitive to the environment. The excitation spectrum of Lu_2O_3:Tb^{3+} (Figure 7b, left) mainly consists of two peaks at 218 and 269 nm, which are assigned to the Lu_2O_3 host absorption and f−d energy transfer in Tb^{3+}, respectively. Upon excitation at 269 nm, the emission spectrum (Figure 7b, right) consists of a group of lines at 490, 543, 598, 625 nm, which may be ascribed to the $^5D_4-^7F_J$ (J = 6, 5, 4, 3) transitions of the Tb^{3+} ions, respectively.

Figure 8 shows the emission spectra, quantum yields (QYs), and absorption coefficients (ACs) of hollow Lu_2O_3:Ln spheres, nanosolid Lu_2O_3:Ln particles, and the bulk Lu_2O_3:Ln phosphors,

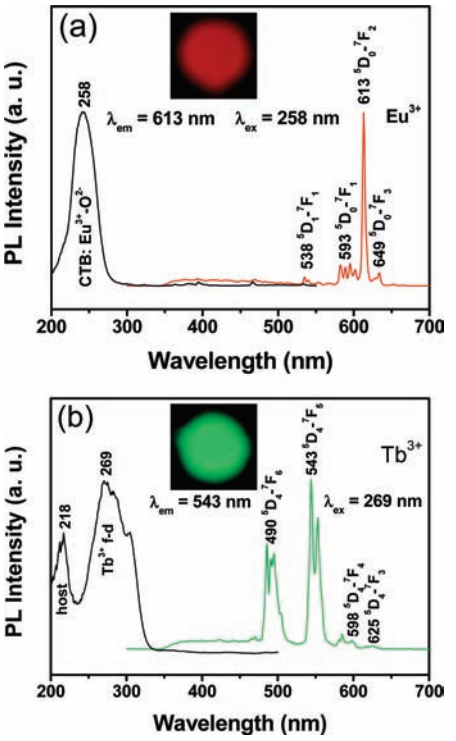

Figure 7. Excitation (left) and emission (right) spectra of hollow Lu_2O_3:Eu^{3+} (a) and Lu_2O_3:Tb^{3+} (b) spheres. (inset) Corresponding photographs under 254 nm UV irradiation.

respectively. In Figure 8a for Lu_2O_3:Eu^{3+}, except for a decrease of the intensity, the emission spectrum of hollow Lu_2O_3:Eu^{3+} spheres is very similar to those of nanosolid Lu_2O_3:Eu^{3+} particles and bulk Lu_2O_3:Eu^{3+} phosphors due to their same f−f transitions which are strongly shielded by the outside 5s and 5p electrons. Furthermore, the absolute QY values of hollow Lu_2O_3:Eu^{3+} spheres, nanosolid Lu_2O_3:Eu^{3+} particles, and the bulk Lu_2O_3:Eu^{3+} phosphors are measured to be 19.8%, 21.9%, and 28%, respectively. And the absorption coefficients of the corresponding samples obtained from UV−visible diffuse reflectance spectra are 4%, 6%, and 8%, respectively. As for Lu_2O_3:Tb^{3+} (Figure 8b), the emission spectrum of hollow Lu_2O_3:Tb^{3+} spheres is also much similar to those of corresponding nanosolid particles and bulk phosphors. The respective QY value of hollow Lu_2O_3:Tb^{3+} spheres, nanosolid Lu_2O_3:Tb^{3+} particles, and the bulk Lu_2O_3:Tb^{3+} phosphors are measured to be 4.4%, 5.6% and 5.8%, while the AC values of the corresponding samples are estimated to be 17%, 31%, and 42%, respectively.

The representative decay curves for the luminescence of Eu^{3+} in hollow Lu_2O_3:Eu^{3+} spheres and Tb^{3+} in hollow Lu_2O_3:Tb^{3+} spheres are presented in Figure 9, respectively. The luminescence decay curves for $^5D_0-^7F_2$ (613 nm) of Eu^{3+} and $^5D_4-^7F_5$ (543 nm) of Tb^{3+} can be well fitted into single-exponential function as $I(t) = A\exp(-t/\tau)$ (where τ is the 1/e lifetime of Ln^{3+} ions). The average lifetimes of Eu^{3+} and Tb^{3+} can be determined to be 1.46 ms for hollow Lu_2O_3:Eu^{3+} and 0.47 ms for hollow Lu_2O_3:Tb^{3+} spheres, respectively. These results are basically in accordance with the literature.[22b]

The CL emission of hollow Lu_2O_3:Eu^{3+} microspheres (Figure 10a) is nearly identical to the PL emission when the accelerating voltage and filament current are fixed at 5 kV and 105 mA. Figure 10b exhibits the intensities of the CL spectra for

dx.doi.org/10.1021/ic101605k |Inorg. Chem. 2011, 50, 2182–2190

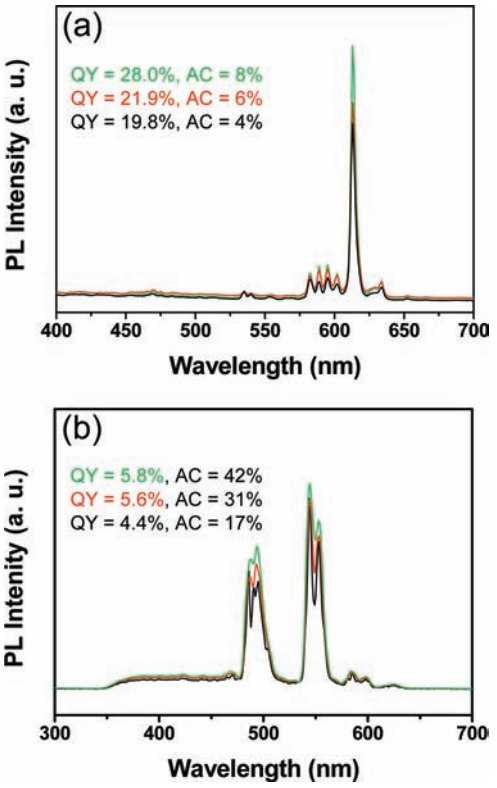

Figure 8. Emission spectra of $Lu_2O_3:Eu^{3+}$ (a) and $Lu_2O_3:Tb^{3+}$ (b): hollow Lu_2O_3:Ln spheres (black line), nanosolid Lu_2O_3:Ln particles (red line), and bulk Lu_2O_3:Ln phosphors (green line). Quantum yields (QYs) and absorption coefficients (ACs) of the corresponding samples are given by different colors in the figure.

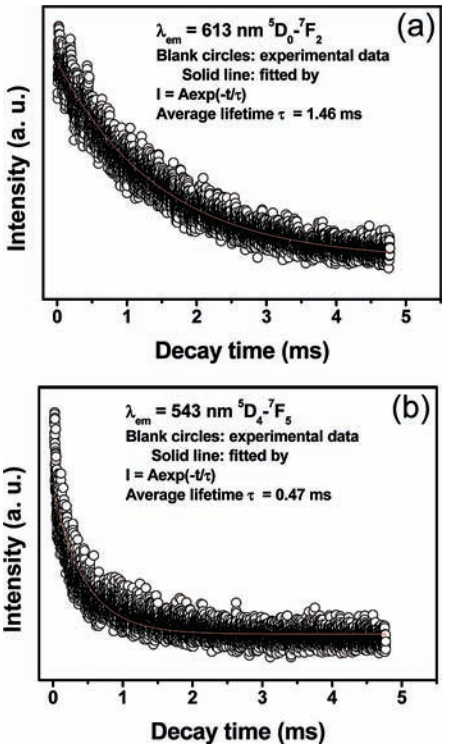

Figure 9. Decay curves for $Lu_2O_3:Eu^{3+}$ (a) and $Lu_2O_3:Tb^{3+}$ (b) spheres.

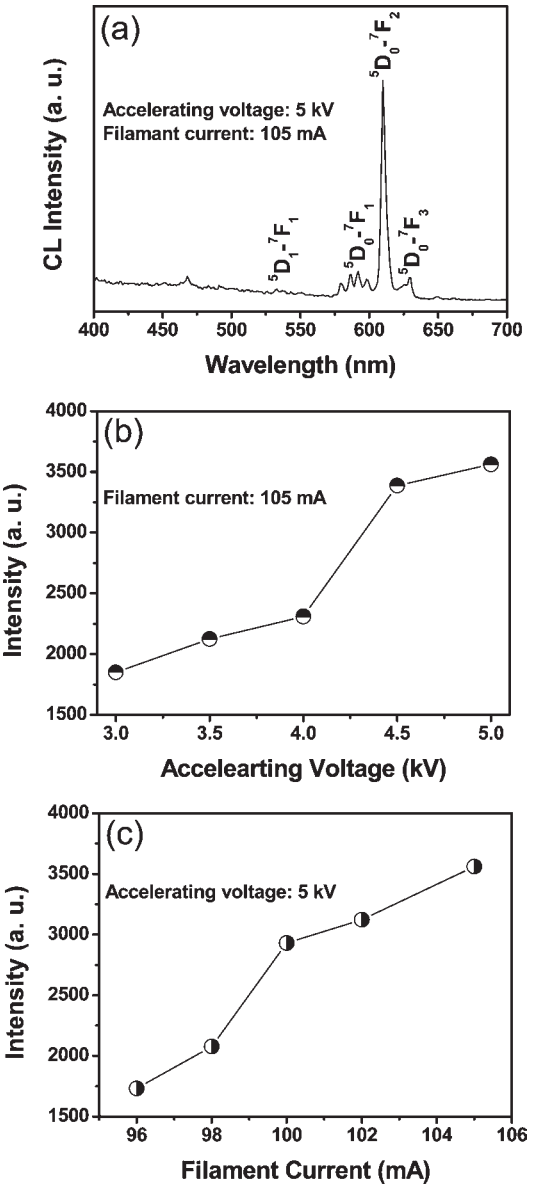

Figure 10. CL spectrum of hollow $Lu_2O_3:Eu^{3+}$ spheres (a) and CL intensity of hollow $Lu_2O_3:Eu^{3+}$ spheres as a function of accelerating voltage (b) and filament current (c).

hollow $Lu_2O_3:Eu^{3+}$ spheres as a function of the accelerating voltage from 3.0−5.0 kV when the filament current is fixed at 105 mA. It can be seen that the emission intensity increases with the accelerating voltage, which can be attributed to the deeper penetration of electrons into the phosphors and the larger electron beam current density. When the accelerating voltage is fixed at 5 kV, the CL intensity shows the similar increasing trend with the filament current from 96 to 105 mA (Figure 10c). The CL properties of hollow $Lu_2O_3:Tb^{3+}$ spheres are given in Figure 11. Much similar results are obtained to those of hollow $Lu_2O_3:Eu^{3+}$ spheres. The electron penetration depth can be estimated by the empirical formula $L[\text{Å}] = 250(A/\rho)(E/Z^{1/2})^n$, where $n = 1.2/(1 - 0.29 \log Z)$, A is the atomic weight, ρ is the density, Z is the atomic number, and E is the accelerating voltage (kV).[26] Hence, either the increase of the accelerating voltage or the filament current can bring deeper penetration of electrons into the phosphors. Accordingly, more plasma will be produced,

dx.doi.org/10.1021/ic101605k |Inorg. Chem. 2011, 50, 2182–2190

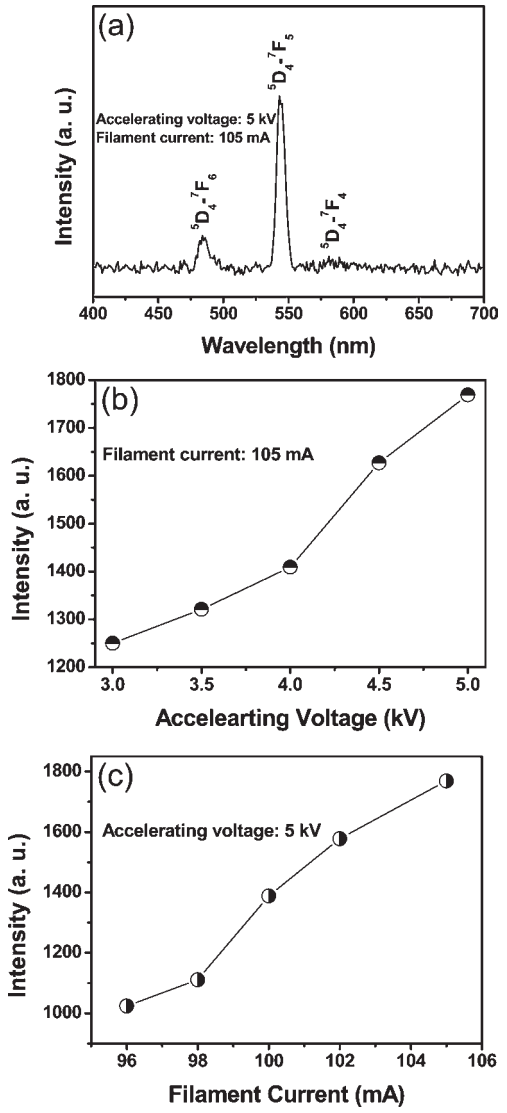

Figure 11. CL spectrum of hollow Lu_2O_3:Tb^{3+} spheres (a) and CL intensity of hollow Lu_2O_3:Tb^{3+} spheres as a function of accelerating voltage (b) and filament current (c).

resulting in more Ln^{3+} ions being excited, and the cathodoluminescent intensity is therefore increased.

3.3. Formation Process. The possible mechanism of the evolution from glucose to carbon spheres and to the final hollow Lu_2O_3:Ln spheres is proposed based on the XRD, FE-SEM, TEM and FT-IR results, as shown in Scheme 1. The formation of hollow Lu_2O_3:Ln spheres may experience three stages. First, uniform carbon sphere templates were obtained by the polymerization of glucose molecules and further dehydration of cross-linked polymer by thermal treatment. In the second step, the core−shell structured precursor was fabricated by the homogeneous precipitation of rare earth ions on the surface of spherical carbon templates using urea as the precipitating agent. FT-IR confirms the presence of abundant hydroxyl groups on the carbon spheres, which is beneficial to the adsorption of Lu^{3+}, Eu^{3+}, OH^-, and CO_3^{2-} (released from precipitator agent urea). The adsorbed components may easily precipitate on the surface of the carbon spheres, then form amorphous $Lu(OH)CO_3$ nucleus and further grow into $Lu(OH)CO_3$ nanoparticles.

Scheme 1. Schematic Illustration for the Formation of Carbon Spheres, Core−Shell Structured Precursor, and Final Hollow Lu_2O_3:Ln Spheres

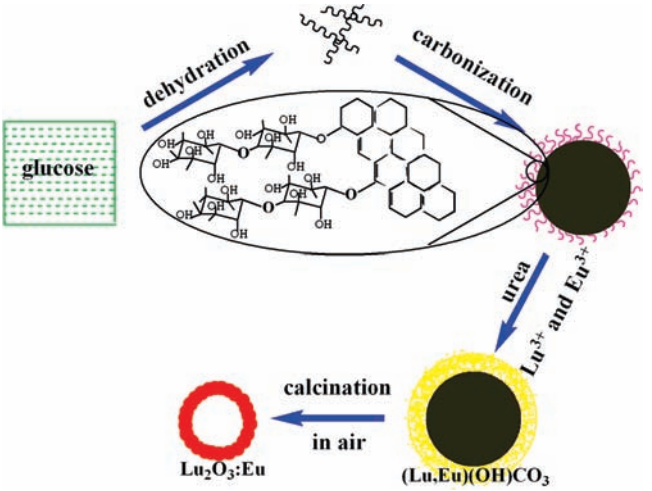

Finally, the carbon sphere templates were burned out and $Lu(OH)CO_3$ particles were decomposed into Lu_2O_3:Ln crystals by the heating treatment, thus uniform hollow Lu_2O_3:Ln spheres were obtained. The main reaction process for the formation of hollow Lu_2O_3:Eu^{3+} spheres (stoichiometric formula: $Lu_{1.9}Eu_{0.1}O_3$) could be represented as follows.

$$CO(NH_2)_2 + H_2O \leftrightarrow CO_2 + 2NH_3 \quad (1)$$

$$NH_3 + H_2O \leftrightarrow NH_4^+ + OH^- \quad (2)$$

$$(95\%Lu^{3+},\ 5\%Eu^{3+}) + 3OH^- + CO_2 \Rightarrow (Lu_{0.95},\ Eu_{0.05})(OH)CO_3 + H_2O \quad (3)$$

$$2(Lu_{0.95},\ Eu_{0.05})(OH)CO_3 \Rightarrow Lu_{1.9}Eu_{0.1}O_3 + H_2O + 2CO_2 \quad (4)$$

4. CONCLUSIONS

In summary, we have demonstrated the fabrication of hollow Lu_2O_3:Ln spheres by a facile sacrifice template method. In the coating process, the slow decomposition of urea resulted in the effective and homogeneous precipitation of rare earth based composite precursor on the surface of carbon spheres. The subsequent calcination brought about the highly crystalline Lu_2O_3:Ln spheres and the removal of carbon template at desired temperature. The hollow microstructured phosphors demonstrate the strong emissions under ultraviolet−visible light excitation. Furthermore, no organic template and corrosively leaching agents were used in the whole fabrication process, and the approach is simple and completely green. The current method is suitable for inexpensive, mass production of hollow Lu_2O_3:Ln phosphors. The synthetic principle should be potential for the synthesis of other uniform, hollow spherical materials.

AUTHOR INFORMATION

Corresponding Author
*E-mail: jlin@ciac.jl.cn.

■ ACKNOWLEDGMENT

This project is financially supported by National Basic Research Program of China (2007CB935502, 2010CB327704), the National Natural Science Foundation of China (NSFC 20871035, 50702057, 50872131), China Postdoctoral Special Science Foundation (200808281), and Harbin Sci.-Tech. Innovation Foundation (No. 2009RFQXG045).

■ REFERENCES

(1) (a) Alivisatos, A. P. *Science* **1996**, *271*, 933.(b) Klabunde, K. J. *Nanoscale Materials in Chemistry*; Wiley-Interscience: New York, 2001.

(2) (a) Arnal, P. M.; Comotti, M.; Schüth, F. *Angew. Chem., Int. Ed.* **2006**, *45*, 8224. (b) Cheng, F.; Ma, H.; Li, Y.; Chen, J. *Inorg. Chem.* **2007**, *46*, 788. (c) Kim, S.-W.; Kim, M.; Lee, W. Y.; Hyeon, T. *J. Am. Chem. Soc.* **2002**, *124*, 7642. (d) Syoufian, A.; Satriya, O. H.; Nakashima, K. *Catal. Commun.* **2007**, *8*, 755.

(3) (a) Zhu, Y.; Shi, J.; Shen, W.; Dong, X.; Feng, J.; Ruan, M.; Li, Y. *Angew. Chem., Int. Ed.* **2005**, *44*, 5083. (b) Li, Z.-Z.; Wen, L.-X.; Shao, L.; Chen, J.-F. *J. Controlled Release* **2004**, *98*, 245. (c) Cai, Y.; Pan, H.; Xu, X.; Hu, Q.; Li, L.; Tang, R. *Chem. Mater.* **2007**, *19*, 3081.

(4) (a) Xu, X.; Asher, S. A. *J. Am. Chem. Soc.* **2004**, *126*, 7940. (b) Rengarajan, R.; Jiang, P.; Colvin, V.; Mittleman, D. *Appl. Phys. Lett.* **2000**, *77*, 3517. (c) Artemyev, M. V.; Woggon, U.; Wannemacher, R. *Appl. Phys. Lett.* **2001**, *78*, 1032.

(5) (a) Feng, X.; Mao, C.; Yang, G.; Hou, W.; Zhu, J.-J. *Langmuir* **2006**, *22*, 4384. (b) Son, S. J.; Bai, X.; Lee, S. B. *Drug Discov. Today* **2007**, *12*, 657.

(6) (a) Chaturvedi, M.; Shen, Y. L. *Acta Mater.* **1998**, *46*, 4287. (b) Rennel, C.; Rigdahl, M. *Colloid Polym. Sci.* **1994**, *272*, 1111.

(7) Sun, Q.; Deng, Y. *J. Am. Chem. Soc.* **2005**, *127*, 8274.

(8) Cao, A.-M.; Hu, J.-S.; Liang, H.-P.; Wan, L.-J. *Angew. Chem., Int. Ed.* **2005**, *44*, 4391.

(9) (a) Tissot, I.; Reymond, J. P.; Lefebvre, F.; Bourgeat-Lami, E. *Chem. Mater.* **2002**, *14*, 1325. (b) Imhof, A. *Langmuir* **2001**, *17*, 3579.

(10) Rana, R. K.; Mastai, Y.; Gedanken, A. *Adv. Mater.* **2002**, *14*, 1414.

(11) Hu, P.; Yu, L.; Zuo, A.; Guo, C.; Yuan, F. *J. Phys. Chem. C* **2008**, *113*, 900.

(12) Bruinsma, P. J.; Kim, A. Y.; Liu, J.; Baskaran., S. *Chem. Mater.* **1997**, *9*, 2507.

(13) Zhu, G.; Qiu., S; Terasaki, O.; Wei, Y. *J. Am. Chem. Soc.* **2001**, *123*, 7723.

(14) Wang, L.; Sasaki, T.; Ebina, Y.; Kurashima, K.; Watanabe, M. *Chem. Mater.* **2002**, *14*, 4827.

(15) Caruso, F.; Caruso, R. A.; Mohwald, H. *Science* **1998**, *282*, 1111.

(16) (a) Caruso, F.; Caruso, R. A.; Mohwald, H. *Chem. Mater.* **1999**, *11*, 3309. (b) Strandwitz, N. C.; Stucky, G. D. *Chem. Mater.* **2009**, *21*, 4577. (c) Jia, G.; You, H. P.; Song, Y. H.; Huang, Y. J.; Yang, M.; Zhang, H. J. *Inorg. Chem.* **2010**, *49*, 7721. (d) Kawahashi, N.; Persson, C.; Matijevic, E. *J. Mater. Chem.* **1991**, *1*, 577. (e) Strohm, H.; Lobmann, P. *J. Mater. Chem.* **2004**, *14*, 2667.

(17) Bourlinos, A. B.; Karakassides, M. A.; Petridis, D. *Chem. Commun.* **2001**, 1518.

(18) (a) Bai, B.; Wang, P.; Wu, L.; Yang, L.; Chen, Z. *Mater. Chem. Phys.* **2009**, *114*, 26. (b) Nomura, T.; Morimoto, Y.; Ishikawa, M.; Tokumoto, H.; Konishi, Y. *Adv. Powder Technol.* **2010**, *21*, 8. (c) Kim, J. W.; Choi, S. H.; Lillehei, P. T.; Chu, S. H.; King, G. C.; Watt, G. D. *Chem. Commun.* **2005**, 4101. (d) Chang, C.; Kimura, F.; Kimura, T.; Wada, H. *Mater. Lett.* **2005**, *59*, 1037. (e) Zhou, H.; Fan, T.; Zhang, D. *Micropor. Mesopor. Mater.* **2007**, *100*, 322. (f) Titirici, M.-M.; Antonietti, M.; Thomas, A. *Chem. Mater.* **2006**, *18*, 3808.

(19) Wan, S. M.; Guo, F.; Shi, L.; Peng, Y. Y.; Liu, X. Z.; Zhang, Y. G.; Qian, Y. T. *J. Mater. Chem.* **2004**, *14*, 2489.

(20) (a) Yada, M.; Mihara, M.; Mouri, S.; Kuroki, M.; Kijima, T. *Adv. Mater.* **2002**, *14*, 309. (b) Polizzi, S.; Bucella, S.; Speghini, A.; Vetrone, F.; Naccache, R.; Boyer, J. C.; Capobianco, J. A. *Chem. Mater.* **2004**, *16*, 1330. (c) Lu, J.; Takaichi, K.; Uematsu, T.; Shirakawa, A.; Musha, M.; Ueda, K.; Yagi, H.; Yanagitani, T.; Kaminskii, A. A. *Appl. Phys. Lett.* **2002**, *81*, 4324.

(21) (a) Guillot-Noël, O.; Bellamy, B.; Viana, B.; Vivien, D. *Phys. Rev. B* **1999**, *60*, 1668. (b) Moine, B.; Dujardin, C.; Lautesse, H.; Pedrini, C.; Combes, C. M.; Belski, A.; Martin, P.; Gesland, J. Y. *Mater. Sci. Forum* **1997**, *239*−*241*, 245. (c) Capobianco, J. A.; Vetrone, F.; Boyer, J. C.; Speghini, A.; Bettinelli, M. *Opt. Mater.* **2002**, *19*, 259.

(22) (a) Jia, G.; Zheng, Y.; Liu, K.; Song, Y.; You, H.; Zhang, H. *J. Phys. Chem. C* **2008**, *113*, 153. (b) Yang, J.; Li, C.; Quan, Z.; Zhang, C.; Yang, P.; Li, Y.; Yu, C.; Lin, J. *J. Phys. Chem. C* **2008**, *112*, 12777.

(23) Pradhan, A. K.; Zhang, K.; Mohanty, S.; Dadson, J.; Hunter, D.; Loutts, G. B.; Roy, U. N.; Cui, Y.; Burger, A.; Wilkerson, A. L. *J. Appl. Phys.* **2005**, 97.

(24) Si, R.; Zhang, Y.-W.; Zhou, H.-P.; Sun, L.-D.; Yan, C.-H. *Chem. Mater.* **2007**, *19*, 18.

(25) Sun, X.; Li, Y. *Angew. Chem., Int. Ed.* **2004**, *43*, 597.

(26) Feldman, C. *Phys. Rev.* **1960**, *117*, 455.